IEEE Access
Multidisciplinary | Rapid Review | Open Access Journal

Received November 7, 2019, accepted November 22, 2019, date of publication December 2, 2019,
date of current version December 13, 2019.

*Digital Object Identifier 10.1109/ACCESS.2019.2957133*

# Design and Analysis of Brushless Wound Field Synchronous Machine With Electro-Magnetic Coupling Resonators

**XINGHE FU, (Member, IEEE), QI QI, (Member, IEEE), AND LINLIN TAN, (Member, IEEE)**
School of Electrical Engineering, Southeast University, Nanjing 210096, China

Corresponding author: Xinghe Fu (fuxinghe@seu.edu.cn)

This work was supported in part by the National Natural Science Foundation of China under Grant 51977035.

**ABSTRACT** The increasing price of rare earth permanent magnet has refocused the attentions to substitute Permanent Magnet Synchronous Machine (PMSM) with Wound Field Synchronous Machine (WFSM), which needs an excitation device to deliver current to the field winding. This paper presents one solution transferring the excitation power into the winding on the rotor of WFSM via electro-magnetic coupling resonance. Analysis, design, and prototype construction of the system are presented. Experiments demonstrate the system can transfer 200W to the field winding of a 2kW WFSM and the overall excitation device efficiency can reach 85%. The proposed technique has unique advantages over other wireless power transfer excitation technologies.

**INDEX TERMS** Wound field synchronous machine, brushless excitation, wireless power transfer, electro-magnetic coupling resonance.

## I. INTRODUCTION

Permanent Magnet Synchronous Machine (PMSM) became an optimal choice for traction applications due to its high torque density [1]. However, the cost of PMSM has greatly increased due to the significant increase in the price of rare earth materials. To some extent, the cost of permanent magnet accounts for almost 50% to 70% of the total cost. However, the cost structure of the Wound Field Synchronous Machine(WFSM) does not depend on the price of rare earth materials. Therefore, it is possible that WFSM becomes a prime candidate for lots of applications. WFSM has several advantages. Its safety and fault tolerance are higher than permanent magnet motor since the magnetic field can be directly adjustable. The cost of WFSM is low because permanent magnet materials are not required. However, the major issue of WFSM is the unreliability caused by slip rings and brushes.

To solve the above issue, a three-stage synchronous machine has been employed as a generator, which was the original brushless excitation applied for high power in conventional aircrafts [2]. The third harmonic excitation, which induces voltage on the rotor and then provides excitation through rectifier, is also a method for eliminating brushes and slip rings and applied in small-capacity motors [3]. Different from third harmonic, a method of generating sub-harmonic and using special inverter control technology to provide excitation is also proposed [4]. A developed brushless self-excitation synchronous generator model is proposed in [5]. The self-excitation consists of residual magnetic force and rises through the interaction between armature reaction field and flux induced by auxiliary rotor winding, which is proportional to the load changes, without any additional excitation device. A novel brushless excitation concept with a rotating power converter is proposed in [6]. An inverter with a DC link capacitor and a controller are added on the rotor and the inverter is controlled such that the alternating current charges the DC link capacitor. Arranging the excitation winding on the stator is an approach that does not need to consider the brushes and slip rings [7]. The DC field excitation windings are placed on the stator with armature windings, and there are no coils or permanent magnets on their rotors. However, this inevitably increases the design difficulty of the stator.

Two new methods, which retaining the structure of the conventional WFSM stator and rotor and implementing brushless excitation by adding an excitation device, have been proposed. One solution is to utilize a rotating transformer to provide excitation current [8], [9], which has been demonstrated that the system efficiency is above 90%.

The associate editor coordinating the review of this manuscript and approving it for publication was Tariq Masood.

The capacitive noncontact power transfer technique proposed by Prof. Ludois in [10], is the second method without brushes and slip rings. Qualitative comparisons between capacitive power transform system and traditional contactless power transfer approaches indicate that the former may be more competitive [11]. Rotary transformers and capacitive slip rings provide two excitation methods, and there is no mechanical contact between the moving part and the stationary part. The rotary transformers inevitably require additional copper and magnetic steel, and speed sensitivity and reliability remain a problem. Capacitive slip rings satisfy this but still have lower power density and complicated structure problems.

An emerging method to deliver power is electro-magnetic coupling resonant Wireless Power Transfer (WPT). In 2007, MIT used a self-resonant coil in a coupled state, and experimentally demonstrated that it can transmit 60W power when the distance is as high as 8 times the coil radius and about 2 meters, and the efficiency can reach 40% [12]. From then on, WPT technique via coupled magnetic resonance has developed rapidly and is widely used in electromobile [12]–[15], health, medical treatment, communication, phone and other applications [17], [18]. Recently, this innovative technique has been applied to WFSM to reduce the overall size and weight [19]. Reference [20] has designed different types of resonators for different excitation demands and calculated the spatial distribution of the excitation magnetic field. Unfortunately, there are no experiment results. Reference [21] has analyzed WPT for motor electric excitation from the perspective of primary-side current control without the analysis of the impact on the motor. Applying coupled magnetic resonance WPT technology to WFSM does not increase the design difficulty of the stator and rotor compared to harmonic excitation and stator wound field synchronous machine. Moreover, no magnetic steel is required on excitation device compared with rotary transformer and the transmission distance can be selected in a wide range compared with rotary transformer and capacitive slip rings.

On the basis of previous research [20], the authors of this article continue to investigate electro-magnetic coupling resonant technique to feed excitation power into the field winding and verify the analytical analysis and design results by some experiments. The simulation and experimental results of brushless WFSM and conventional brush WFSM are given and compared with each other. In this paper, section II describes the structure, the operating principle and the characteristic of the brushless WFSM system. Section III gives the design process and design results of the brushless WFSM. Section IV analyzes the resonance characteristics under variable load and gives the design basis. Section V highlights experimental work and makes comparison.

## II. STRUCTURE AND CHARACTERISTIC OF BRUSHLESS WFSM SYSTEM

The stator and rotor structure of the proposed machine remain same as that of a conventional brush WFSM, and the only

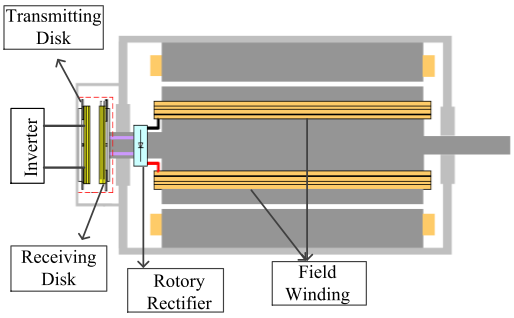


**FIGURE 1.** Profile view of WFSM equipped with WPT assembly.

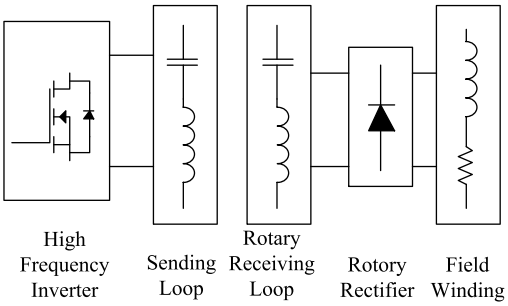


**FIGURE 2.** Simplified circuit for WPT system.

difference between the conventional synchronous and modified WFSM is the excitation device. The excitation device of a conventional synchronous machine involves brushes and slip rings. While in the brushless WFSM, a WPT excitation device takes its place. A pair of resonators and a rotary rectifier are designed to replace the slip rings to transmit power to exciting winding. The mechanical structure has high integrity as illustrated in Fig.1. The device consists of five parts, including the power supply, high frequency inverter, resonator (transmitting and receiving resonator disks), uncontrolled rectifier, and load (field winding). There is no mechanical contact between the sending and receiving disks. The high frequency inverter and sending resonator disk are stationary component placed at the end of the generator. Receiving resonator disk and the rectifier are placed on the rotor shaft and rotate with the rotor.

The simplified circuit of the excitation power transmission system is shown in Fig.2, the power is transmitted by the magnetic coupling between the transmitting and the receiving resonant disks, and the frequency of the high frequency inverter coincides with the self-resonant frequency of the resonator. A resonant tank is formed by connecting an inductor coil and a capacitor in series. Two resonant tanks are utilized in the WPT excitation device, and the inductors and capacitors on the two resonant tanks are the same. Connected to the high frequency inverter is the transmitting resonant tank, and the rectifier and the load are connected to the receiving tank. Relative motion is allowed when the relative surface area and the distance between the two tanks keep the same. Then the two resonant tanks realize wireless power transmission via electro-magnetic coupling.

**TABLE 1. Parameters of the WFSM.**

| Symbol | Quantity |
|---|---|
| Number of Poles | 4 |
| Rated Power/ kW | 2 |
| Rated Field Current / A | 3.6 |
| Stator OD/ mm | 210 |
| Stator ID/ mm | 150 |
| Rotor OD/ mm | 149 |
| Stack Length/ mm | 105 |
| Stator Turns Per Slot | 44 |
| Number of Slot | 36 |
| Resistance of Field Winding/Ω | 15 |
| Inductance of Field Winding/ mH | 400 |

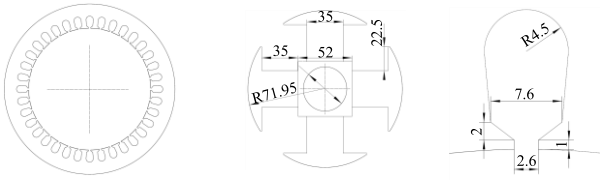


**FIGURE 3. (a) Geometric model of WFSM stator, (b) rotor and (c) stator slot.**

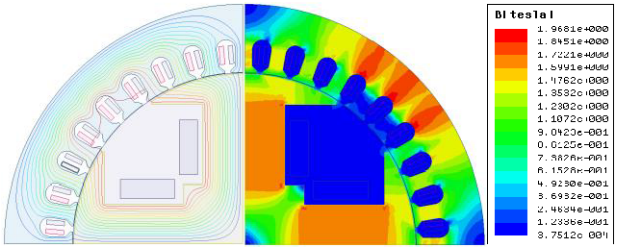


**FIGURE 4. Magnetic field line and magnetic density by FEM.**

Table 1 shows the parameters and main dimensions of the WFSM. The geometric model of the stator and rotor are shown in Fig.3.

Fig.4 shows the magnetic field line and magnetic density distribution of half model by FEM. Fig.5 shows the back EMF of the machine in the case of 3.6 A excitation current and 200 r/min. And the amplitude of back EMF of the WFSM is 40V.

## III. ELECTRO-MAGNETIC COUPLING RESONANCE DESIGN

### A. ELECTRICAL PARAMETERS OF RESONANT COILS

A simplified WPT system, which treats the supply as an ideal high-frequency power source, is utilized. As shown in Fig.6, we assume that the coupled resonant circuit is driven by a square waveform $u_s$. In the coupled resonant tanks, $L_1$ and $L_2$ are effective inductances, $C_1$ and $C_2$ are effective capacitances, $R_1$ and $R_2$ are equivalent series resistances, $M$ is mutual inductance, $C$ is filter capacitor, and $L$ is load inductance and $R$ is load resistance. $u_s$ is regarded as supply source.

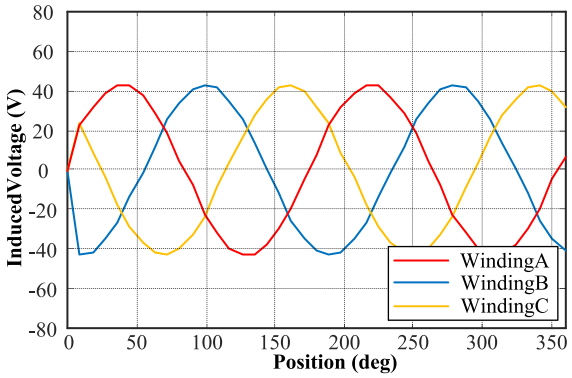


**FIGURE 5. Back EMF with a field current of 3.6A and 200r/min.**

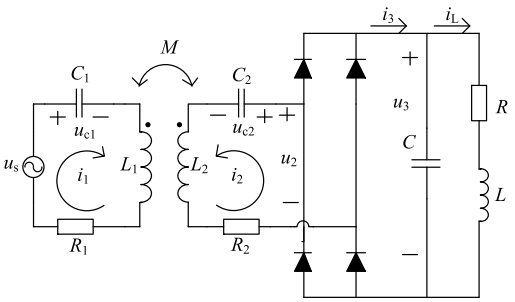


**FIGURE 6. Circuit diagram of the magnetic coupling resonant WPT.**

**TABLE 2. Parameters of the coupling resonant WPT system.**

| Symbol | Parameter | Quantity |
|---|---|---|
| $L_1$ | Inductance of sending coil/μH | 100 |
| $L_2$ | Inductance of receiving coil/μH | 100 |
| $C_1$ | Capacitance of sending coil/ nF | 412 |
| $C_2$ | Capacitance of receiving coil/ nF | 412 |
| $f$ | Resonant frequency/kHz | 25 |

It is assumed that the effective value and angular frequency of the current flowing through the coil are $I_{\rm rms}$ and $\omega$, the inductive reactive power is

$$Q = \omega L_{1,2} I_{rms}^2 \tag{1}$$

It can be seen from Table 1 that the WPT excitation device is designed to provide 3.6A excitation current and 200W power. High working frequency could cause electromagnetic interference problem and iron loss in ferrous-metallic structures. Therefore, a relatively suitable resonant frequency of 25 kHz is chosen.

Thereby, the calculated resonant inductance of 100$\mu$H is selected to transmit required power, and the required resonant capacitance calculated according to (2) is 412nF. The parameters of the resonant tanks as the excitation device are shown in Table 2.

$$C_{1,2} = \frac{1}{(2\pi f)^2 \cdot L_{1,2}} \tag{2}$$

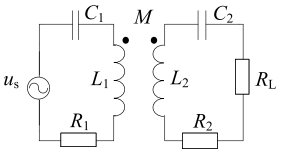


**FIGURE 7.** Equivalent circuit of two-coils structure.

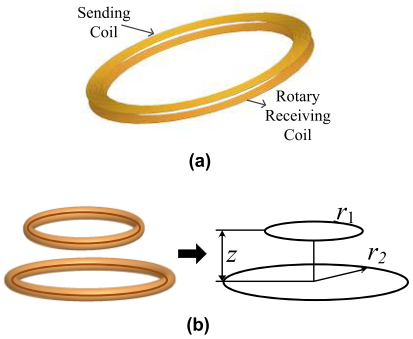


**FIGURE 8.** (a)Planar spiral coils model; (b) Circular concentric filaments.

### B. STRUCTURE PARAMETERS OF RESONANT COILS

The load current is the main concern when the field winding of the WFSM acts as load on the electro-magnetic coupling resonator. The series-series topology is selected because of its constant current characteristics, as illustrated in Fig.7. It should be pointed out that an equivalent resistor $R_{\mathrm{L}}$ can be utilized instead of the entire field winding load.

A planar spiral coil is designed to transfer excitation current to the rotor for its advantages in axial length as shown in Fig.8. The self-inductance of the planar spiral coil can be calculated using the filament method [22], [23], which applying only to circular filaments of negligible cross section. The formulas of self-inductance and mutual inductance are expressed as follows:

$$M_{ij} = \frac{2\mu_0\sqrt{r_i r_j}}{k}[(1-\frac{k^2}{2})K(k) - E(k)] \tag{3}$$

$$k^2 = \frac{4r_i r_j}{(r_1+r_2)^2+z^2} \tag{4}$$

$$L_1 = \sum_{i=0}^{N_1-1}\sum_{j=0}^{N_1-1} M_{ij},\ z=0 \quad L_2 = \sum_{i=0}^{N_2-1}\sum_{j=0}^{N_2-1} M_{ij},\ z=0 \tag{5}$$

$$M = \sum_{i=0}^{N_1-1}\sum_{j=0}^{N_2-1} M_{ij} \tag{6}$$

where, $M_{\mathrm{ij}}$ is the mutual inductance between two filaments, $r_{\mathrm{i}}$ and $r_{\mathrm{j}}$ are radii of the filaments respectively and $z$ is the distance between the centers of the two filaments, $E$ and $K$ are complete elliptic integrals of the first and second kind, respectively, $\mu_0$ is vacuum permeability. $N_1$ and $N_2$ are the number of turns and $r_{\mathrm{i}} = r_{\mathrm{inner}} + d/2{+}s*i$, $r_{\mathrm{j}} = r_{\mathrm{inner}} + d/2{+}s*j$.

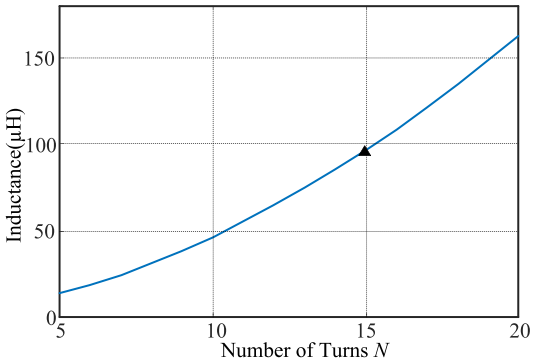


**FIGURE 9.** Self-inductance as function of number of turns.

Assuming that a copper wire having a diameter of $d = 1$mm is selected, the inner radius of the coil is $r_{\mathrm{inner}} = 92.5$mm and the radii of two adjacent filaments differs by $s = 1.15$mm.

The relationship between the self-inductance and the number of turns is as shown in Fig.9.

When $N = 15$, the required resonant inductor can be obtained. The parameters of the transmitting coil and the receiving coil are the same. Ignoring the loss of the power supply, the efficiency $\eta_{2C}$ of two-coils WTP system is expressed as follow [24]:

$$\eta_{2C} = \frac{(\omega M)^2 \cdot R_L}{(R_2+R_L)[R_1(R_2+R_L)+(\omega M)^2]} \tag{7}$$

$R_1$ and $R_2$ are equivalent resistances of transmitting coil and receiving coil and their resistance values are usually small and similar. Therefore, it can be seen from the expression that at a given frequency, load and mutual inductance are the main factors affecting efficiency. And the mutual inductance is mainly determined by the transmission distance and decreases as the distance increases.

By measurement, $R_1 = R_2 = 0.3\Omega$. Then, according to equation (7), the efficiency of the two-coils system as a function of equivalent resistance and mutual inductance is shown in Fig.10.

It is obvious that the two-coils structure can obtain higher efficiency when transmitting with large load for a short distance. In this paper, the equivalent resistance $R_{\mathrm{L}}$ is about $14\Omega$ by measurement. As can be seen from Fig.10, the transmission distance can be selected in a relatively wide range since the mutual inductance is inversely proportional to transmission distance. When the mutual inductance is $60\mu$H, 96% efficiency can be achieved. Then, according to the previous calculation, $M = 60\mu$H when $z = 12$mm. At last, the parameters of the spiral coils are shown in Table 3.

## IV. RESONANT CHARACTERISTICS UNDER VARIABLE LOAD

The field winding of WESM is a kind of resistive-inductive load. Moreover, its inductance value would change due to the saturation of the magnetic circuit. WPT technique has been

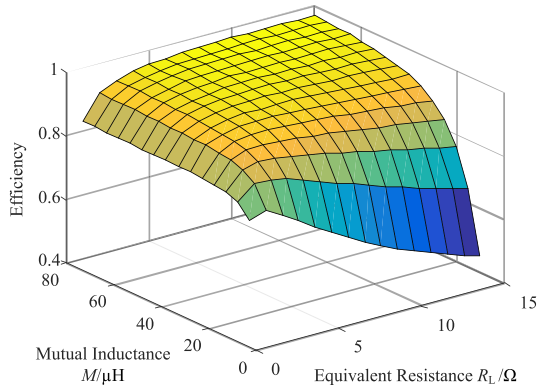


**FIGURE 10.** Efficiency variation of two-coils structures.

**TABLE 3.** The parameters of the sprial coils.

| Symbol | Parameter | Quantity |
|---|---|---|
| $r_{out\_1}$, $r_{out\_2}$ | Outer radii of coils/ mm | 110 |
| $r_{in\_1}$, $r_{in\_2}$ | Inner radii of coils/ mm | 92.5 |
| $d_1$, $d_2$ | Copper diameter/ mm | 1 |
| $N_1$, $N_2$ | Number of turns | 15 |
| $z$ | Distance between two coils/ mm | 12 |

studied a lot, but in most studies, power is transferred to a resistive load. There are relatively less researches on the effect of load impedance on resonant characteristics. This paper establishes a state space model of the magnetic coupling resonant WPT system that exactly represents the model dynamics and explores the effects on resonant frequency.

In Fig. 6, the relationship between $i_3$ and $i_2$ is given by

$$\begin{cases} i_3 = i_2 & i_2 \geq 0 \\ i_3 = -i_2, & i_2 < 0 \end{cases} \tag{8}$$

The equivalent circuit dynamics can be completely defined by the spatial state space model as follows

$$\begin{aligned} \frac{di_1}{dt} &= \frac{1}{L_1L_2 - M^2}[-L_2R_1i_1 - L_1u_{c1} + MR_2i_2 \\ &\quad + Mu_{c2} + Msgn(i_2)u_3 + L_2u_s] \\ \frac{di_2}{dt} &= \frac{1}{L_1L_2 - M^2}[MR_1i_1 + Mu_{c1} - L_1R_2i_2 \\ &\quad - L_1u_{c2} - L_1sgn(i_2)u_3 - Mu_s] \\ \frac{du_{c1}}{dt} &= \frac{1}{C_1}i_1, \quad \frac{du_{c2}}{dt} = \frac{1}{C_2}i_2 \\ \frac{du_3}{dt} &= \frac{1}{C}[sgn(i_2)i_2 - i_L], \quad L\frac{di_L}{dt} = u_3 - Ri_L \end{aligned} \tag{9}$$

The circuit model in this paper has a filter capacitor and an inductor connected to the rectifier bridge, that is, the equivalent impedance after the rectifier bridge has an imaginary part, which is different from the pure resistive load system. The equivalent load after the rectifier bridge can be regarded as a series-parallel connection of capacitor, inductor and resistor. As shown in Fig. 6, the equivalent impedance is

$$Z_{eq} = \frac{(R + j\omega L) \cdot \frac{1}{j\omega C}}{R + j\omega L + \frac{1}{j\omega C}} \tag{10}$$

By expanding the above formula, the imaginary part can be obtained as

$$Im = \frac{\omega[L - \omega^2L^2C - CR^2]}{(1 - \omega^2LC)^2 + (\omega CR)^2} \tag{11}$$

It can be seen that the imaginary part of the equivalent impedance is determined by the value of $R$, $L$, $C$ and the frequency of the current $\omega$. As can be seen from Table 2, $L_1 = L_2 = 100\mu$H, $C_1 = C_2 = 412$nF, $f = 25$ kHz. In addition, $R_1 = R_2 = 0.3\Omega$, $M = 60\mu$H. In order to analyze the effect of impedance characteristics on resonance, this paper assumes that $u_s = 45$V, this numerical assumption does not affect the characteristics of the system under study.

It should be pointed that the impedance characteristics of the load are not taken into account when selecting the parameters of the resonant disk. Based on the spatial state equation established above, this paper explores the effects of $R$, $L$ and $C$ on the resonance respectively.

As shown in Fig.11 (a), $L = 40$mH, $C = 40\mu$F, the shift of the resonant frequency caused by the change of the resistance within a certain range is very small. The current is slightly heading the voltage when the resistance increases. However, Fig.11 (b) shows that the effect of the filter capacitor on the resonance is slightly larger than the resistance when keep $R = 15\Omega$, $L = 40$mH. When $C = 0.2\mu$F, the current lags behind the voltage, while the current slightly exceeds the voltage when capacitance reaches $40\mu$F. In Fig.11(c), $C = 40\mu$F, $R = 15\Omega$, it can be seen that the inductance has little effect on the resonance over a relatively large range. In summary, $R$, $L$, and $C$ all have a more or less effect on resonance, but their effects are negligible, and the inductance and capacitance can be tolerated over a considerable range. This feature allows the inductance to change and the transmission characteristics are not disturbed.

## V. EXPERIMENTAL RESULTS AND COMPARISON

### A. PROTOTYPE AND EXPERIMENTAL SETUP

The instrument involved in this experiment had a frequency converter, a servo motor, a modified WFSM, a conventional brush WFSM, two designed resonant disks, a rectifier with MUR420RLG diodes, a high frequency inverter, a DC source, a three-phase adjustable resistive load, and an oscilloscope. The modified WFSM acted as a generator, in which slip ring was replaced with resonant disks and rectifier, and the servo motor as prime motor drove the conventional WFSM and the modified brushless WFSM respectively. The experimental principle is shown in Fig. 12.

Fig.13 shows the final modified motor-generator setup with WPT excitation device installed on shaft and some components. The WFSM shaft end was extended with a rubber block, and the receiving resonant coil and resonant capacitor

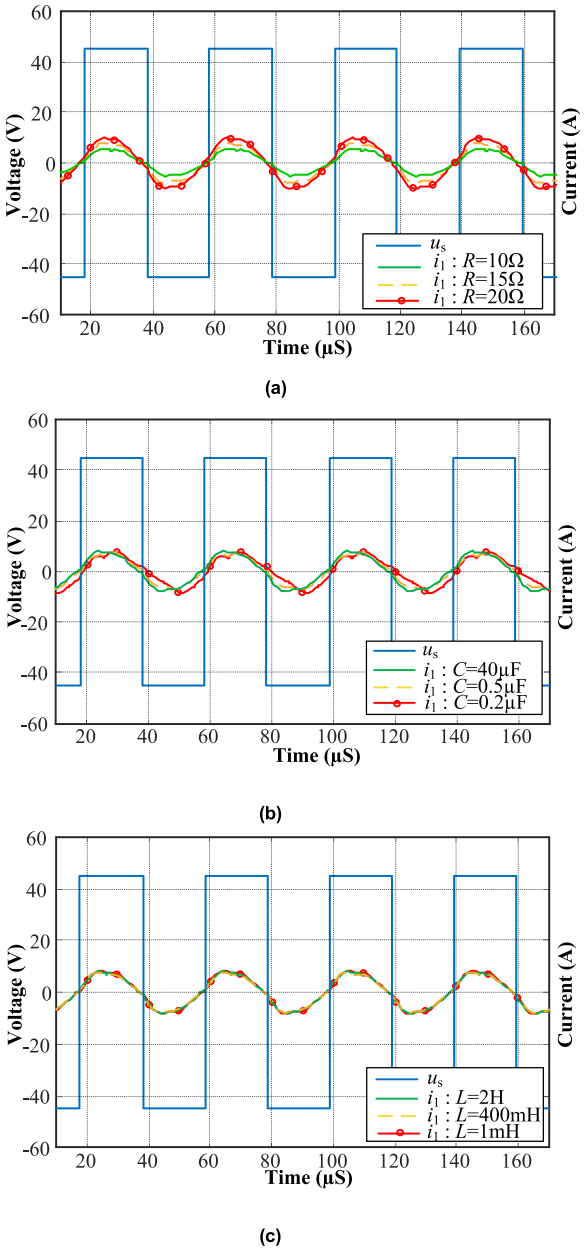


**FIGURE 11.** Calculated data plots of $u_s$ and $i_1$ (a) at $L$ = 40mH, $C$ = 40$\mu$F; (b) at $R$ = 15Ω, $L$ = 40mH; (c) at $C$ = 40$\mu$F, $R$ = 15Ω.

were fixed on a circular acrylic plate and mounted on the rubber block. The transmitting disk was symmetrically placed and connected to the inverter power supply. To measure the excitation current and receiving coil voltage, the auxiliary brushes are installed on the stator and the auxiliary slip rings are installed on rotor, which are described in Fig 13 (a). One group of brushes and slip rings are parallel connected with the rectifier. Another group of brushes and slip rings are series connected in the excitation circuit. The detail parameters of the WFSM are shown in Table 1 and the dominant resonator configurations are presented in Table 2. Static and rotary experiments were performed to verify the WPT excitation device.

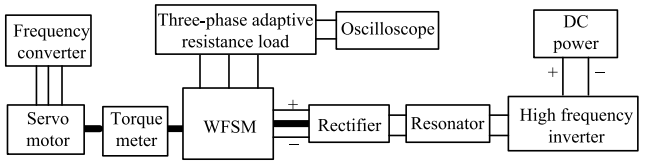


**FIGURE 12.** Experimental principle.

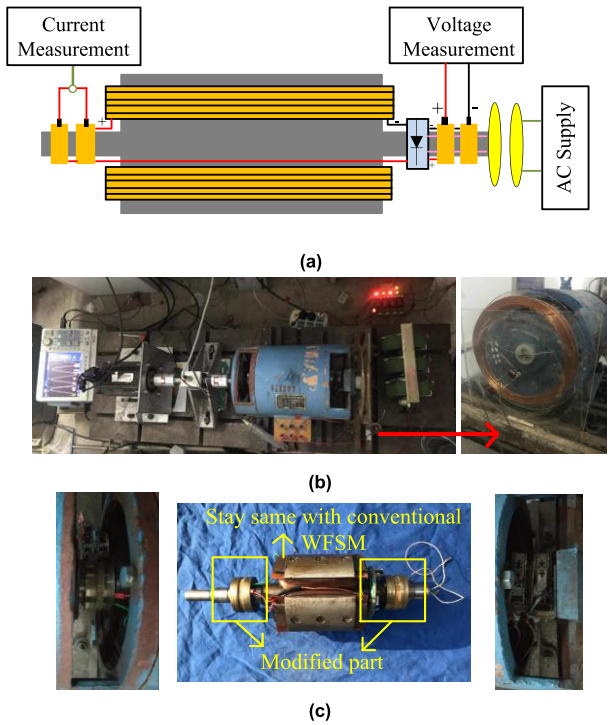


**FIGURE 13.** Prototype and wiring diagram (a) Model diagram; (b) Experimental motor-generator setup with WPT excitation device; (c) Modified rotor and brush and slip rings.

### *B. STATIONARY EXPERIMENT RESULTS AND ANALYSIS*

System efficiency can be measured in static experiments. At the same time, simulation in Matlab-Simulink is used to compare with the experimental process.

Terminal quantities $u_1$, $i_1$, $u_2$, $i_2$ under stationary conditions are plotted in Fig.14. The high frequency inverter outputs a 45V, 25 kHz frequency square wave voltage to obtain an excitation current of 3.6A. The energy distribution is obtained by measuring the voltages and currents of each port under the static experiment, as shown in Fig.15. The distortion of the current on the transmitting coil and the receiving coil is due to the strong coupling between the inductors, and increasing the distance can reduce the distortion, but inevitably reduce the transmission efficiency.

### *C. ROTARY EXPERIMENT RESULTS AND ANALYSIS*

#### 1) NO-LOAD EXPERIMENT

In order to compare the performance of the modified WFSM with the conventional WFSM, the original WFSM with brushes and slip rings was drove by the servo motor, and

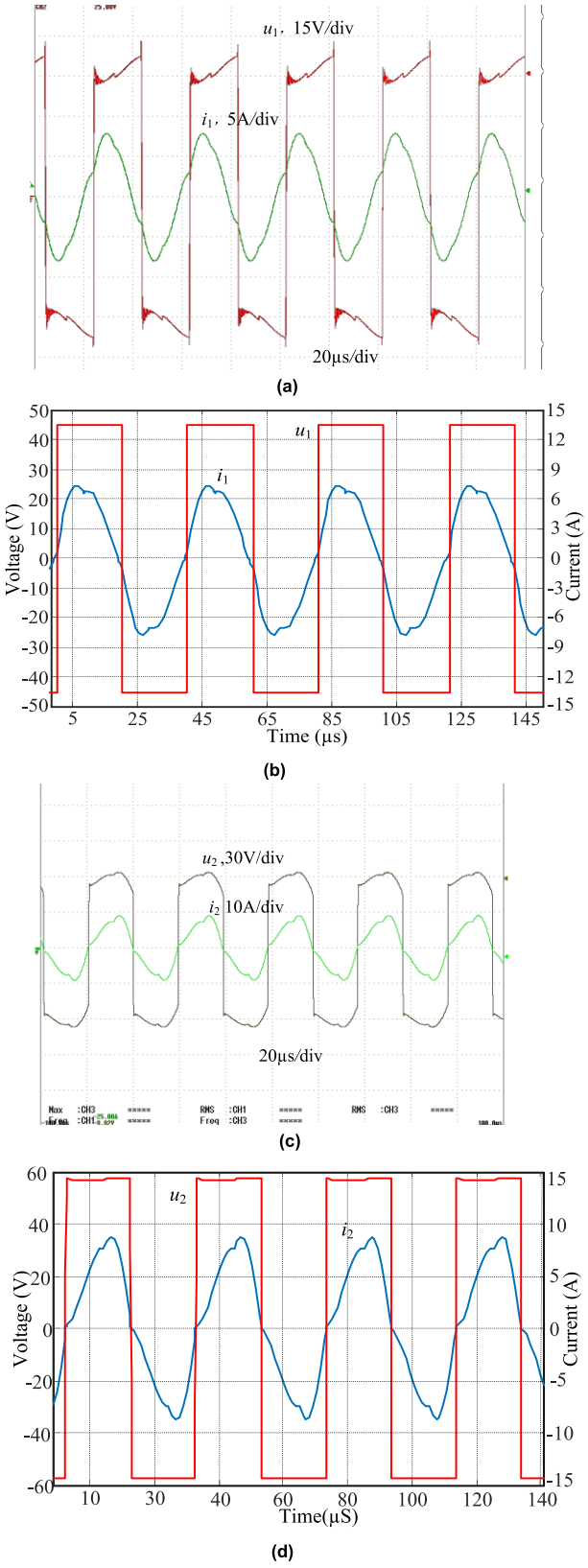


**FIGURE 14.** (a) Experimental data plot of $u_1$ and $i_1$; (b) Simulated data plot of $u_1$ and $i_1$; (c) Experimental data plot of $u_2$ and $i_2$; (d) Simulated data plot of $u_2$ and $i_2$.

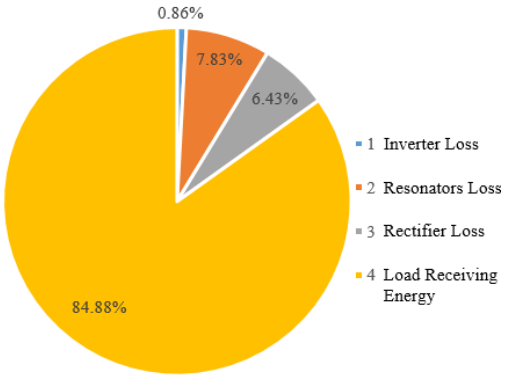


**FIGURE 15.** Energy distribution of static experiment at 3.6A excited current.

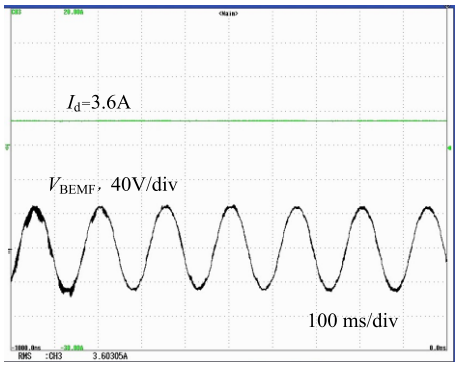


**FIGURE 16.** Experimental Back EMF $v_{BEMF}$ and field current $I_d$.

the experimental speed of the original WFSM was consistent with that of the brushless WFSM. The rotary experiment measured the Back-EMF of the brush WFSM and brushless WFSM under different excitation current, respectively. As can be seen from Fig. 13 (a), the excitation current can still be measured while the rotor was rotating.

The Back-EMF of the original brush and brushless WFSMs and excitation current $i_f$ are obtained under rotary experiments and shown in Fig.16, which is basically consistent with finite element analysis results.

The comparison of measured Back-EMF between the original brush and brushless WFSM is presented in Fig.17. It is obvious that the two curves are extremely consistent. Furthermore, the relationship between the supply $u_s$ and excitation current $i_f$ is given in Fig.18. $u_s$ and $i_f$ are almost proportional, adjusting the $i_f$ only requires adjusting the $u_s$.

### 2) LOAD EXPERIMENT

In order to investigate the external characteristic of the brushless WFSM, a three-phase adjustable resistive load is connected to the brushless WFSM in a star connection, and the three-phase adjustable resistor ranges from 50Ω to 100Ω. Fig.19 shows the phase voltage $U$ and phase current $I$ of

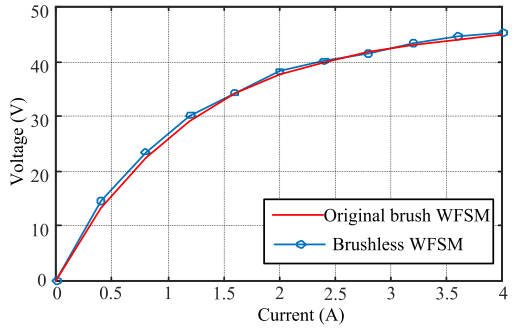


**FIGURE 17.** Experimental Back EMF as function of field current at 200r/min.

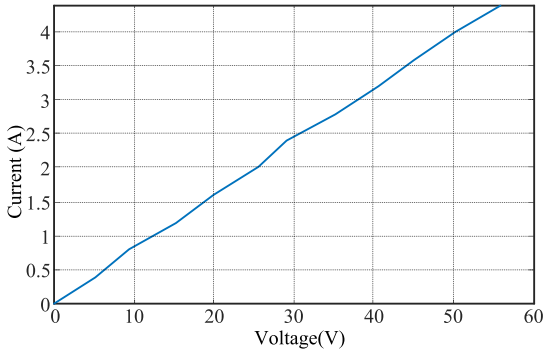


**FIGURE 18.** Experimental brushless WFSM field current $i_f$ as function of DC supply voltage $v_{dc}$.

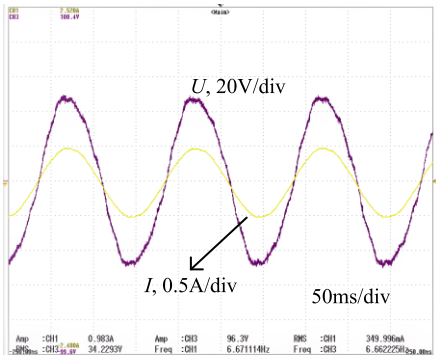


**FIGURE 19.** Experimental phase voltage and phase current of the brushless WFSM for each phase with a resistance of 100Ω at 200r/min.

the brushless WFSM with a resistance of 100Ω at 200r/min, which is limited by the mechanical strength of the modified equipment.

The mechanical power input to the brushless WFSM measured by torque and speed meter is 50W. Therefore, the efficiency of the brushless WFSM is about 70% according to the phase voltage and current. The efficiency is consistent with the original brush WFSW with a resistance of 100Ω at 200r/min. It can be foreseen that the load characteristics of the brushless WFSM and the original brush WFSM are the same as long as the excitation device works normally, because the

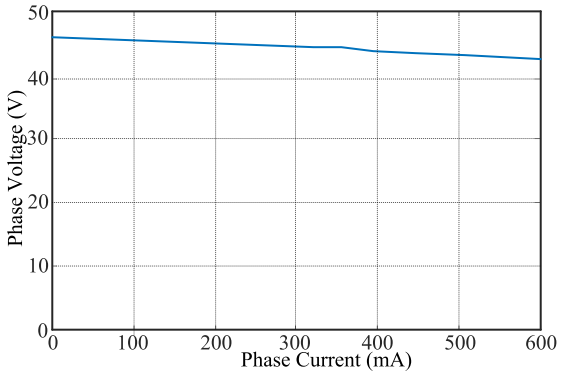


**FIGURE 20.** Experimental external characteristic of the brushless WFSM at power factor of 1.

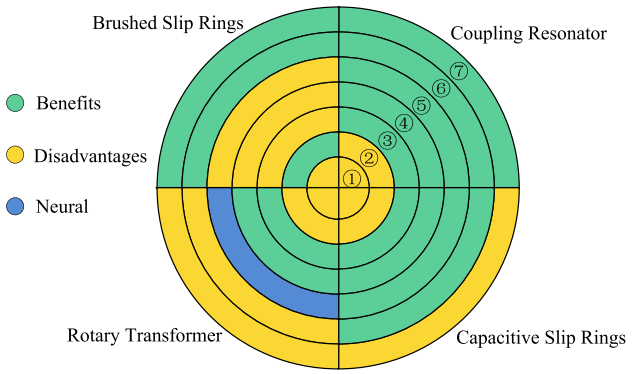


**FIGURE 21.** Comparisons between available solutions for WFSMs.

two WFMSs have the same parameters except the excitation mode.

The external characteristics of the brushless WFSM at power factor of 1 can be obtained by changing the value of the three-phase adjustable resistive load, as shown in Fig.20. The external characteristic is degraded due to the demagnetization of the armature reaction and the leakage impedance drop.

Whether the excitation device can transmit the required excitation current effectively and stably is the focus of this paper. The load characteristic with a power factor of 1 has verified that the excitation device can still work stably when the brushless WFSM is loaded.

## VI. CONCLUSION

This paper proposes a brushless field excitation system for WFSM based on electro-magnetic coupling resonance technique. Analysis, design, and prototype construction of the system are presented. Experiments show that the system can

transfer 200 W to the field winding of a 2 kW WFSM. Additional qualitative comparisons between an electromagnetic coupling resonance WPT exciting method and other wireless power transmission methods are drawn in Fig.21.

The main conclusions and contribution are as follows:

1) Considering the high price and scarcity of rare earth materials, the excitation method based on electromagnetic coupling resonance is feasible and alternative to PM machines.

2) Although the field winding is an inductive load, its effects can be negligible. This feature allows the inductance to change and the transmission characteristics are not disturbed.

3) The efficiency of overall excitation device can reach 85%, which means that the proposed excitation method is competitive.

4) Load current can be adjusted directly and simply through power supply thanks to the constant current characteristics of the resonator's topology.

In spite of significant progress has been made of brushless excitation technique in WFSM, there are still many issues to be addressed in the future:

1) The effect of high-frequency magnetic field on the frame, end winding, shaft, and etc. and impact of metal obstacles on WPT system should be further studied.

2)The excitation method based on electro-magnetic coupling resonators has potential in power transmission and structure, but electromagnetic loss and stability consideration have not been studied and remain to further investigate.

## REFERENCES

[1] J. A. Krizan and S. D. Sudhoff, "A design model for salient permanent-magnet machines with investigation of saliency and wide-speed-range performance," *IEEE Trans. Energy Convers.*, vol. 28, no. 1, pp. 95–105, Mar. 2013.

[2] Z. Zhang, W. Liu, D. Zhao, S. Mao, T. Meng, and N. Jiao, "Steady-state performance evaluations of three-phase brushless asynchronous excitation system for aircraft starter/generator," *IET Elect. Power Appl.*, vol. 10, no. 8, pp. 788–798, Sep. 2016.

[3] F. Yao, Q. An, X. Gao, L. Sun, and T. A. Lipo, "Principle of operation and performance of a synchronous machine employing a new harmonic excitation scheme," *IEEE Trans. Ind. Appl.*, vol. 51, no. 5, pp. 3890–3898, Sep./Oct. 2015.

[4] Q. Ali, T. A. Lipo, and B. I. Kwon, "Design and analysis of a novel brushless wound rotor synchronous machine," *IEEE Trans. Magn.*, vol. 51, no. 11, pp. 1–4, Nov. 2015.

[5] L. F. A. Izzat and S. Heier, "Development in design of brushless self-excited and self-regulated synchronous generator," in *Proc. Int. Conf. Renew. Energy Res. Appl. (ICRERA)*, Madrid, Spain, Oct. 2013, pp. 1024–1029.

[6] J. Pötter, M. Pfost, and G. Schullerus, "A novel brushless excitation system for synchronous machines with a rotating power converter," in *Proc. IEEE 13th Int. Conf. Compat., Power Electron. Power Eng. (CPE-POWERENG)*, Sonderborg, Denmark, Apr. 2019, pp. 1–6.

[7] Z. Q. Zhu, Y. J. Zhou, J. T. Chen, and J. E. Green, "Investigation of nonoverlapping stator wound-field synchronous machines," *IEEE Trans. Energy Convers.*, vol. 30, no. 4, pp. 1420–1427, Dec. 2015.

[8] C. Stancu, T. Ward, K. Rahman, R. Dawsey, and P. Savagian, "Separately excited synchronous motor with rotary transformer for hybrid vehicle application," *IEEE Trans. Ind. Appl.*, vol. 54, no. 1, pp. 223–232, Jan. 2018.

[9] D. Bortis, L. Fässler, A. Looser, and J. W. Kolar, "Analysis of rotary transformer concepts for high-speed applications," in *Proc. 28th Annu. IEEE Appl. Power Electron. Conf. Exposit. (APEC)*, Long Beach, CA, USA, Mar. 2013, pp. 3262–3269.

[10] J. Dai, S. Hagen, D. C. Ludois, and I. P. Brown, "Synchronous generator brushless field excitation and voltage regulation via capacitive coupling through journal bearings," *IEEE Trans. Ind. Appl.*, vol. 53, no. 4, pp. 3317–3326, Jul. 2017.

[11] D. C. Ludois, J. K. Reed, and K. Hanson, "Capacitive power transfer for rotor field current in synchronous machines," *IEEE Trans. Power Electron.*, vol. 27, no. 11, pp. 4638–4645, Nov. 2012.

[12] O. Jonah and S. V. Georgakopoulos, "Wireless power transfer in concrete via strongly coupled magnetic resonance," *IEEE Trans. Antennas Propag.*, vol. 61, no. 3, pp. 1378–1384, Mar. 2013.

[13] G. A. J. Elliott, J. T. Boys, and A. W. Green, "Magnetically coupled systems for power transfer to electric vehicles," in *Proc. Int. Conf. Power Electron. Drive Syst. (PEDS)*, Singapore, Feb. 1995, pp. 797–801.

[14] D. Patil, M. K. McDonough, J. M. Miller, B. Fahimi, and P. T. Balsara, "Wireless power transfer for vehicular applications: Overview and challenges," *IEEE Trans. Transport. Electrific.*, vol. 4, no. 1, pp. 3–37, Mar. 2018.

[15] J. M. Miller and A. Daga, "Elements of wireless power transfer essential to high power charging of heavy duty vehicles," *IEEE Trans. Transport. Electrific.*, vol. 1, no. 1, pp. 26–39, Jun. 2015.

[16] M. Bojarski, E. Asa, K. Colak, and D. Czarkowski, "Analysis and control of multiphase inductively coupled resonant converter for wireless electric vehicle charger applications," *IEEE Trans. Transport. Electrific.*, vol. 3, no. 2, pp. 312–320, Jun. 2017.

[17] T. Campi, S. Cruciani, and M. Feliziani, "Wireless power transfer technology applied to an autonomous electric UAV with a small secondary coil," *Energies*, vol. 11, no. 2, pp. 352-1–352-15, Feb. 2018.

[18] H. Liu, L. Tan, and X. Huang, M. Zhang, Z. Zhang, and J. Li, "Power stabilization based on switching control of segmented transmitting coils for multi loads in static-dynamic hybrid wireless charging system at traffic lights," *Energies*, vol. 12, no. 4, p. 607, Feb. 2019.

[19] G. W. Box, "Wound field synchronous machine with resonant field exciter," U.S. Patent 9 525 376 B2. Dec. 20, 2016.

[20] F. Wen, X. Huang, and L. Tan, "A new type of power supply for excitation mechanism of motor in electrical appliance," in *Proc. IEEE PELS Workshop Emerg. Technol., Wireless Power Transf. (WoW)*, Chongqing, China, May 2017, pp. 139–142.

[21] J. Kang, Y. Liu, and L. Sun, "A primary-side control method of wireless power transfer for motor electric excitation," in *Proc. 14th IEEE Conf. Ind. Electron. Appl. (ICIEA)*, Xi'an, Chinaa, Jun. 2019, pp. 2423–2428.

[22] F. W. Grover, *Inductance Calculations: Working Formulas and Tables*. New York, NY, USA: Dover, 1946.

[23] S. Babic and C. Akyel, "Improvement in calculation of the self- and mutual inductance of thin-wall solenoids and disk coils," *IEEE Trans. Magn.*, vol. 36, no. 4, pp. 1970–1975, Jul. 2000.

[24] Y. Zhang, Z. Zhao, and K. Chen, "Load matching analysis of magnetically-coupled resonant wireless power transfer," in *Proc. IEEE ECCE Asia Downunder*, Melbourne, VIC, Australia, Jun. 2013, pp. 788–792.

**XINGHE FU** (S'09–M'19) received the B.S. degree in electric machines and drives from the Shenyang University of Technology, Shenyang, China, the M.S. degree in control theory and control engineering from Northeast University, Shenyang, and the Ph.D. degree in electric machines and electric apparatus from the Harbin Institute of Technology, Harbin, China. He is currently an Associate Professor with the School of Electrical Engineering, Southeast University, Nanjing, China. His research interests include small and special motors, motor control, and industrial automation.

**QI QI** (S'10–M'19) received the B.S. degree in electrical engineering from the Chongqing University of Posts and Telecommunications, Chongqing, China. She is currently pursuing the master's degree with the School of Electrical Engineering, Southeast University, Nanjing, China. Her research interests include electric machines and wireless power transmission.

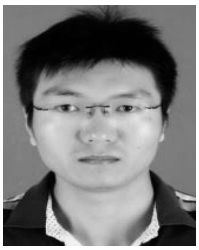

**LINLIN TAN** (S'10–M'19) received the B.S. degree in electrical engineering and automation from Harbin Engineering University, Harbin, China, in 2008, and the Ph.D. degree in electrical engineering from Southeast University, Nanjing, China, in 2014. He is currently an Associate Professor with the School of Electrical Engineering, Southeast University. He has published more than 20 articles. His current research interests include wireless power transfer, wireless charging for electric vehicles, and wireless V2G.